Geophys. J. Int. (2003) **154,** 154–165

Global anisotropic phase velocity maps for fundamental mode surface waves between 40 and 150 s

Jeannot Trampert[1] and John H. Woodhouse[2]

[1] *Faculty of Earth Sciences, Utrecht University,* PO Box 80021,TA 3058 *Utrecht, the Netherlands. E-mail: jeannot@geo.uu.nl*
[2] *Department of Earth Sciences, Oxford University,* 3 *Parks Road, Oxford* OX1 3PR

Accepted 2003 February 10. Received 2003 February 5; in original form 2002 August 28

SUMMARY

We constructed global phase velocity maps including azimuthal anisotropy. Azimuthal anisotropy is expanded on a basis of generalized spherical harmonics, which makes the calculation of path integrals of the phase velocity particularly simple. It is generally accepted that the major difficulty in such modelling is determining the strength of the anisotropy relative to the isotropy. We propose a technique which finds the optimum relative weighting of the anisotropic terms prior to inversion. It is clear from our analyses that phase data require azimuthal anisotropy. We further find that Love wave data do not require a 2ψ term, whereas Rayleigh wave data need 2ψ and 4ψ terms. The main effect of azimuthal anisotropy upon the isotropic maps is a loss of power in the highest spherical harmonic degrees, resulting in an overall lower lateral resolution compared with a purely isotropic inversion for the same number of recovered parameters. The correlation of 2ψ and 4ψ components at different periods is relatively high, indicating a shallow source for the azimuthal anisotropy. Overall, fast 2ψ Rayleigh directions agree well with absolute plate motions in the hotspot reference frame.

Key words: azimuthal anisotropy, inverse theory, phase velocity, surface waves, tomography.

1 INTRODUCTION

It is now well established that the Earth's uppermost mantle is anisotropic. The earliest evidence is the possibility of a discrepancy between the dispersion of Love and Rayleigh waves (Anderson 1961; Harkrider & Anderson 1962) and the azimuthal dependence of oceanic P_n velocities (Hess 1964). Surface waves are particularly well suited to studying anisotropy since they carry information on the radial and azimuthal anisotropy of the upper mantle. Radial anisotropy was first observed when it was established that isotropic velocity models failed to explain simultaneously Love and Rayleigh wave dispersion data (Aki & Kaminuma 1963; McEvilly 1964). This is referred to as the Love–Rayleigh discrepancy and is an indirect observation of anisotropy. A directly observable manifestation of anisotropy is the azimuthal variation of phase velocities, first noticed by Forsyth (1975) in the Pacific Ocean. Since these pioneering studies, many more observations followed and detailed overviews may be found in Anderson (1989), Babuška & Cara (1991) and Montagner (1998). Radial and azimuthal anisotropy in surface waves are the result of the same underlying anisotropy of the Earth's interior, and Montagner & Nataf (1986) linked both together in a common mathematical framework. The theory, initially developed for a flat layered Earth, was later extended to a spherical Earth (Romanowicz & Snieder 1988; Larsen *et al.* 1998).

The necessity for radial anisotropy in the uppermost mantle has never been questioned in reference models (e.g. Dziewonski & Anderson 1981) or 3-D models (e.g. Nataf *et al.* 1984; Ekström & Dziewonski 1998), while global azimuthal phase velocity maps have not been constructed since earlier efforts (e.g. Tanimoto & Anderson 1984, 1985; Montagner & Tanimoto 1990), despite a tremendous increase in high-quality measurements (Trampert & Woodhouse 1995; Ekström *et al.* 1997; van Heijst & Woodhouse 1999) from automatic data processing. There are several reasons for this. Azimuthal anisotropy is assumed to be small compared with radial anisotropy and relevant to this assumption is the increased instability of the inverse problem (Zhang & Lay 1996). Indeed, adding azimuthal anisotropy amounts to adding more parameters to an already underdetermined inverse problem and hence the need for stronger regularization. Modelling shows that the amplitude of the azimuthal terms strongly depends upon damping (e.g. Levshin *et al.* 2001), making it difficult to test the assumption of small azimuthal anisotropy. Furthermore, tests have questioned whether phase data are really sensitive enough to detect azimuthal anisotropy (Larsen *et al.* 1998; Laske & Masters 1998) and the use of additional polarization data has been proposed.

It is certainly worth mapping anisotropy, which can give insight into the convective flow inside the Earth. This connection has been made as early as the 1980s (Regan & Anderson 1984; Tanimoto & Anderson 1984) and since then has been well accepted and put in a

firm mineral physics context (e.g. Karato 1998). If we want to fully understand the anisotropic structure of the Earth, radial anisotropy is not enough, we also need observations of azimuthal anisotropy. The main problem lies in determining the strength of the azimuthal terms. We propose to subject the data to systematic statistical tests to extract this strength prior to constructing the anisotropic phase velocity maps. It is convenient to parametrize the problem in terms of generalized spherical harmonics as shown in the next section. We then explain how we can estimate the strength of the azimuthal terms from the data and discuss the results of our obtained models.

2 PARAMETRIZATION

A plane-layered medium in the presence of a slight general anisotropy gives rise to an azimuthal dependence of the local phase velocity (Smith & Dahlen 1973, 1975). The same azimuthal dependence is found in a spherical Earth (Romanowicz & Snieder 1988; Larsen *et al.* 1998) and we can write

$$\frac{dc}{c}(\omega, \psi) = \alpha_0(\omega) + \alpha_1(\omega)\cos(2\psi) + \alpha_2(\omega)\sin(2\psi) + \alpha_3(\omega)\cos(4\psi) + \alpha_4(\omega)\sin(4\psi), \quad (1)$$

where dc/c is the local relative phase velocity perturbation with respect to a spherically symmetric reference Earth model, ω is the radial frequency and ψ is the azimuth along the path. This can be rewritten as

$$\frac{dc}{c}(\omega, \psi) = \alpha_0(\omega) + \tau_{ij}\nu_i\nu_j + \sigma_{\mathrm{ijkl}}\nu_i\nu_j\nu_k\nu_l, \quad (2)$$

where indices i, j, k, l take values of 1 and 2 corresponding to the co-latitude θ and the longitude ϕ, respectively. $\boldsymbol{\nu} = (-\cos\psi, \sin\psi)$ is a unit vector in the direction of propagation of the surface wave. $\boldsymbol{\tau}$ and $\boldsymbol{\sigma}$ are completely symmetric and trace-free tensors on the 2-D spherical surface and have two independent components given by

$$\tau_{\theta\theta} = -\tau_{\phi\phi} = \alpha_1(\omega) \quad (3)$$

$$\tau_{\theta\phi} = \tau_{\phi\theta} = -\alpha_2(\omega) \quad (4)$$

$$\sigma_{\theta\theta\theta\theta} = -\sigma_{\theta\theta\phi\phi} = \sigma_{\phi\phi\phi\phi} = \alpha_3(\omega) \quad (5)$$

$$\sigma_{\theta\theta\theta\phi} = -\sigma_{\phi\phi\phi\theta} = -\alpha_4(\omega). \quad (6)$$

We can now define the corresponding canonical contravariant spherical components of $\boldsymbol{\tau}$ and $\boldsymbol{\sigma}$ as (Phinney & Burridge 1973)

$$\tau^{++} = \alpha_1(\omega) + i\alpha_2(\omega) \quad (7)$$

$$\tau^{--} = \alpha_1(\omega) - i\alpha_2(\omega) \quad (8)$$

$$\sigma^{++++} = \alpha_3(\omega) + i\alpha_4(\omega) \quad (9)$$

$$\sigma^{----} = \alpha_3(\omega) - i\alpha_4(\omega). \quad (10)$$

All other contravariant components are zero. A simple way to describe azimuthal anisotropy is then to expand τ^{++} and σ^{++++} in terms of generalized spherical harmonics (Phinney & Burridge 1973)

$$\tau^{++} = \sum_{l=2}^{L}\sum_{m=-l}^{l} t_l^m Y_l^{2m}(\theta, \phi) \quad (11)$$

$$\sigma^{++++} = \sum_{l=4}^{L}\sum_{m=-l}^{l} s_l^m Y_l^{4m}(\theta, \phi). \quad (12)$$

Path integrals of dc/c are now readily calculated by making use of spherical harmonic rotation matrices to reduce any path to an equatorial path. The advantages of this parametrization are that there are no singularities in the description associated with the indeterminacy of azimuths at the poles, the inverse problem becomes invariant with respect to rotations of the coordinate system and analytic results are available for the path integrals. The forward problem then reduces to the usual linear relation

$$\mathbf{d} = \mathbf{G}\mathbf{m}, \quad (13)$$

where $\mathbf{d}$ are the path-averaged phase velocity measurements, $\mathbf{m} = (\mathbf{m}_0, \mathbf{m}_2, \mathbf{m}_4)^{\mathrm{T}}$ is the model vector of the spherical harmonic coefficients corresponding to the 0ψ, 2ψ and 4ψ terms, respectively, and $\mathbf{G} = \mathrm{diag}(\mathbf{G}_0, \mathbf{G}_2, \mathbf{G}_4)$ is the block-diagonal matrix of the path-averaged spherical harmonics. $\mathbf{G}_0$ contains the ordinary path-averaged spherical harmonics and $\mathbf{G}_2$ and $\mathbf{G}_4$ correspond to the generalized spherical harmonics defined in eqs. (11) and (12), respectively. The number of unknowns is $(L+1)^2$ for the 0ψ or azimuthally averaged terms, $(2L+6)(L-1)$ for the 2ψ terms and $(2L+10)(L-3)$ for the 4ψ terms. In the following, we use $L = 40$ for the isotropic terms and $L = 20$ for the azimuthal terms, resulting in 3405 unknowns.

3 IS AZIMUTHAL ANISOTROPY REQUIRED?

As mentioned in the introduction, several papers have questioned whether phase data are sufficiently sensitive to azimuthal anisotropy. The main reason for these doubts is the strong dependence of the amplitude of anisotropy upon regularization in the inverse problem. Constructing a global isotropic phase velocity map requires solving a linear inverse problem of several tens of thousands of data and 1681 unknowns for a spherical harmonic expansion up to degree 40. Even though the number of data largely exceeds the number of parameters, errors and inconsistencies in the data and inhomogeneous ray coverage make it impossible to retrieve all model parameters. The inverse problem is unstable and needs to be regularized. Recent maps typically solve for 800 independent parameters out of the 1681 (e.g. Trampert & Woodhouse 2001). Adding azimuthal terms as shown in eq. (1) roughly doubles the number of unknowns without changing the data. The inverse problem becomes more unstable and needs stronger damping. There is no objective criterion for choosing the damping and experience shows that the amplitude of the azimuthal terms depends strongly upon it. On the other hand, adding more parameters into the inversion process generally results in a better variance reduction. The question is then whether the improvement in variance reduction is due to the shear fact of increasing the number of parameters or if the data really prefer azimuthal terms. The answer to this question is given by the F-test (e.g. Bevington & Robinson 1992), which states to what level of confidence the difference in variance reduction is significant.

The inverse problem defined in eq. (14) is solved in the usual way by minimizing a cost function

$$C = (\mathbf{d} - \mathbf{G}\mathbf{m})^{\mathrm{T}}\mathbf{C}_{\mathrm{d}}^{-1}(\mathbf{d} - \mathbf{G}\mathbf{m}) + \mathbf{G}^{\mathrm{T}}\mathbf{C}_m^{-1}\mathbf{m}, \quad (14)$$

where $\mathbf{C}_{\mathrm{d}}$ is the data covariance matrix, which we take to be diagonal and where the data errors have been determined by cluster analyses (Trampert & Woodhouse 2001). $\mathbf{C}_m$ is a diagonal matrix, which

we use to impose smoothness upon the model vector. We prefer Laplacian over model damping to reduce spectral leakage (Trampert & Snieder 1996) and the derivation of the smoothness operator can be found in Trampert & Woodhouse (1995). As the model vector, $\mathbf{C}_m$ is partitioned to emphasize 0ψ, 2ψ and 4ψ terms leading to the explicit expressions

$$(C_{m_0})_{jj} = \frac{1}{\lambda}\frac{1}{[l(l+1)]^2} \tag{15}$$

$$(C_{m_2})_{jj} = \frac{\theta_2}{\lambda}\frac{1}{[l(l+1)]^2} \tag{16}$$

$$(C_{m_4})_{jj} = \frac{\theta_4}{\lambda}\frac{1}{[l(l+1)]^2}, \tag{17}$$

where λ is an overall damping parameter which controls the trade-off between data misfit and smoothness. The smaller its value, the more the model parameters are allowed to vary and the better the data are explained. θ_2 and θ_4 control the relative strength of anisotropy. A uniform value of 0.1, for instance, puts 10 times more signal into the isotropic terms relative to the anisotropic ones. To gain an idea of reasonable values for θ_2 and θ_4, we minimize eq. (14) many times, systematically varying the parameters λ, θ_2 and θ_4 and plot the reduced χ^2 as a function of independent parameters in the final model. To compare two different inversions, the total number of unknowns put in the inverse problem is irrelevant, what matters is the number of independent parameters used to construct the estimated model, given by the trace of the resolution matrix. We define the reduced χ^2 as

$$\chi^2 = \frac{1}{N-M}(\mathbf{d}-\mathbf{Gm})^{\mathrm{T}}\mathbf{C}_{\mathrm{d}}^{-1}(\mathbf{d}-\mathbf{Gm}), \tag{18}$$

where N is the number of data and $M = \mathrm{trace}(\mathbf{R})$. The obtained misfit curves show which parametrization explains the data best for a given number of independent parameters. A standard F-test tells us further how significant the differences between two given curves are.

Before turning to real data, we would like to comment on several synthetic tests. We calculated synthetic data with randomly generated isotropic and anisotropic models using our Love wave data coverage (Fig. 1). We added errors drawn from a Gaussian distribution with a standard deviation of 10 per cent of the values of the synthetic data. First, we inverted data corresponding to a purely random isotropic model of spherical harmonic degree 40 (1681 unknowns). The misfit curves are shown in Fig. 2(a). Clearly, the isotropic description (small θ_2 and θ_4) explains the data much better for any given number of independent parameters and as we reduce the overall damping λ (i.e. allow more parameters in the inversion) χ^2 monotonically tends towards 1. The higher the strength of the anisotropic terms, the higher χ^2 for a given number of independently resolved parameters, because fewer isotropic parameters are available to explain the data. The F-test shows that the differences between all the misfit curves are 100 per cent significant. We then inverted data corresponding to a purely random 2ψ and 4ψ anisotropic model of spherical harmonic degree 20 (874 2ψ and 850 4ψ coefficients). As expected, the inversion with the highest emphasis on anisotropy has the smallest χ^2 (Fig. 2b) for any given trace of the resolution. The F-test shows again that the differences between all the misfit curves are 100 per cent significant. It is further seen in Fig. 2(b) that a mainly isotropic model can explain the anisotropic data to some extent. This has been remarked before (e.g. Larsen *et al.* 1998) and is due to inherent trade-offs between the isotropic and anisotropic terms. This trade-off which depends on the data coverage is not severe in our case because of the complementary azimuthal coverage of major and minor arc data (Fig. 1). Consequently, the χ^2 of the isotropic model tends asymptotically towards the large value of 20, whereas including reasonable strengths of anisotropy makes the χ^2 tend towards 1. In previous anisotropic phase velocity reconstructions it has been noted that Love data show a strong 2ψ term (Montagner & Tanimoto 1990). This is quite puzzling because a general slightly anisotropic medium should give rise to small 2ψ Love terms only (Montagner & Nataf 1986). Such reasoning assumes self-coupling and a good candidate to explain the discrepancy would be to evoke strong Love–Rayleigh coupling. Before complicating the theoretical framework, however, we want to make sure that our data coverage can distinguish between 2ψ and 4ψ models. We thus generated a random 4ψ-only degree-20 model (850 model parameters) and calculated various misfit curves (Fig. 2c). Sure enough the misfit curve corresponding to a suppressed 2ψ inversion gives the smallest misfit. Allowing 2ψ terms in the inversion increases the misfit. The F-test assigns 100 per cent significance to the differences up to the first 850 parameters. Beyond 850 parameters we are running out of 4ψ parameters and some signal is explained by 2ψ parameters, bringing the misfit curves closer together. Repeating the same test for a purely 2ψ input model results in the smallest misfit for a mainly 2ψ inversion. These calculations indicate that we have the possibility to determine the strength of azimuthal anisotropy from the data and that the data coverage is sufficient to distinguish between the different azimuthal terms. It should be noted, however, that in these synthetic tests all parameters were completely controlled, particularly, the size and distribution of the uncertainties was perfectly known. In the case of real data this is clearly more difficult.

4 MISFIT CURVES FOR THE DATA

We generated as outlined above misfit curves for our data. The most difficult part in the measuring process is to assign errors to the data because many assumptions are implicit in such measurements. We found that a reliable estimate was derived from cluster analyses when we included measurements made with varying assumptions (Trampert & Woodhouse 2001). Errors assigned by cluster analyses assume a Gaussian distribution, which is difficult to check in most cases. Consequently, errors in the data are only approximately known compared with the perfectly determined synthetic tests and make it difficult to distinguish between some misfit curves. Examples of the results are seen in Figs 3 and 4. In general, for small numbers of inverted parameters (long-wavelength or low spherical harmonic degree inversions), purely isotropic parametrizations explain the data best. Allowing more parameters in the inversion, eventually anisotropic models become more efficient in explaining the data. Part of the smaller-scale isotropic structure is, in fact, due to long-scale anisotropic structure. This is similar to the textbook example of a finely layered isotropic medium which behaves as a transversely isotropic medium when overall apparent elastic properties are considered. From approximately 500 parameters onwards, we gain at least 5 per cent in χ^2 reduction if we allow some azimuthal anisotropy, indicating that the data clearly contain anisotropic information. The F-test shows that this is significant with 100 per cent confidence. Looking closer, there are also differences in the misfit curves between different strengths of anisotropy although much smaller than compared with the isotropic case. The question

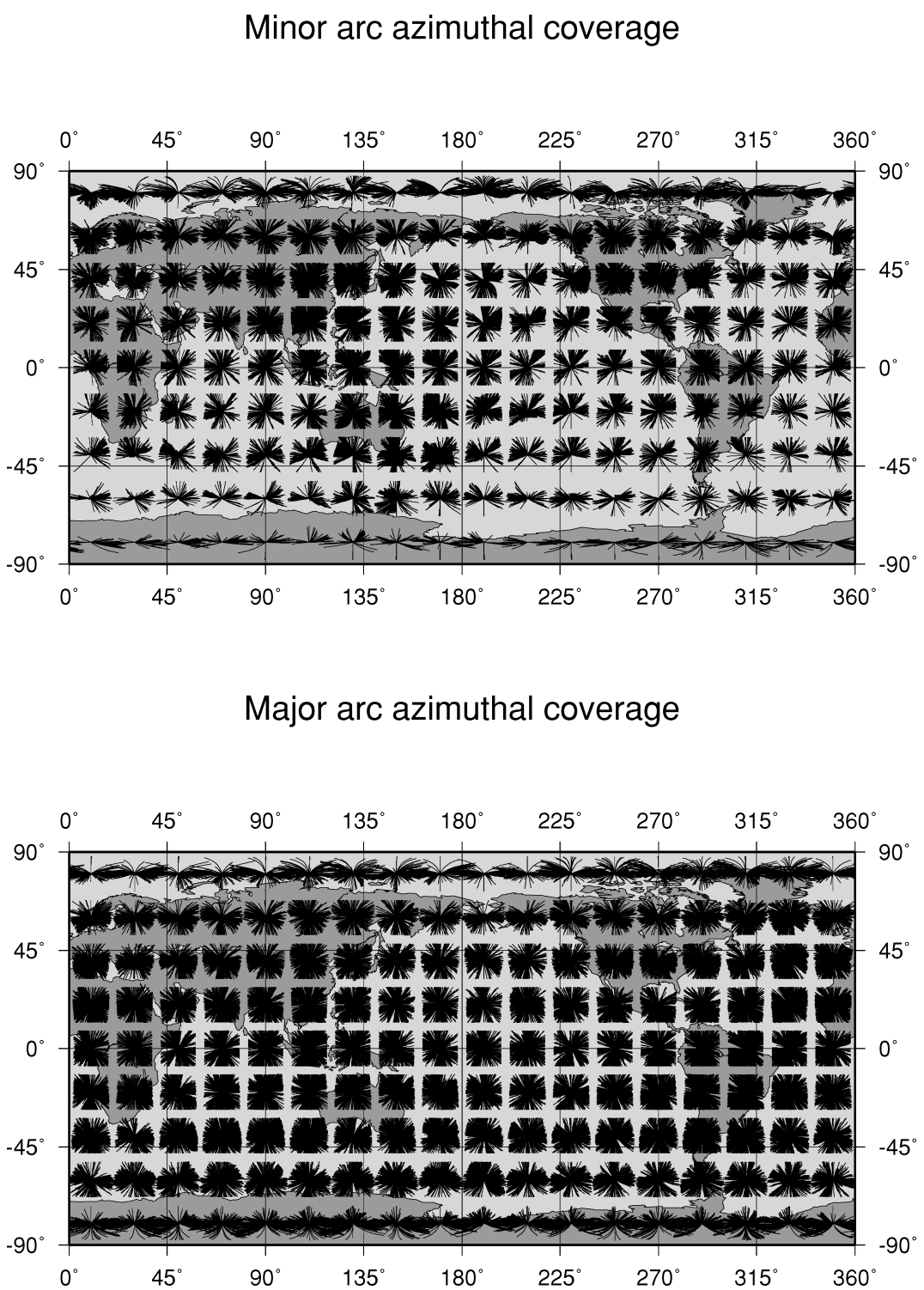

Figure 1. Azimuthal coverage of Love wave rays calculated for 20×20 deg^2 cells. Top: azimuthal coverage for minor arcs. Bottom: azimuthal coverage for major arcs. Note how the major arcs fill important gaps in the azimuthal coverage of the minor arcs. Using minor arcs alone could thus lead to biases in the azimuthal terms. The averaged ray density per cell (not shown) is high and relatively uniform between 1000 and 10 000 rays per cell for a total of 58 506 paths.

is whether or not these differences are significant. The significance varies as a function of inverted parameters and the eigenvalue spectra corresponding to the inverse problem indicate that roughly 800 independently inverted parameters are a reasonable choice for our Love and Rayleigh wave coverage (see also Trampert & Woodhouse 2001).

For Love waves, all anisotropic misfit curves (Fig. 3) are close together and the F-test shows that for 800 free parameters, there is at least a 30 per cent chance (up to 80 per cent depending on period) that the differences are not significant. Note that we included misfit curves for 4ψ azimuthal terms only to test whether or not our data require 2ψ terms. This is an important question because a general

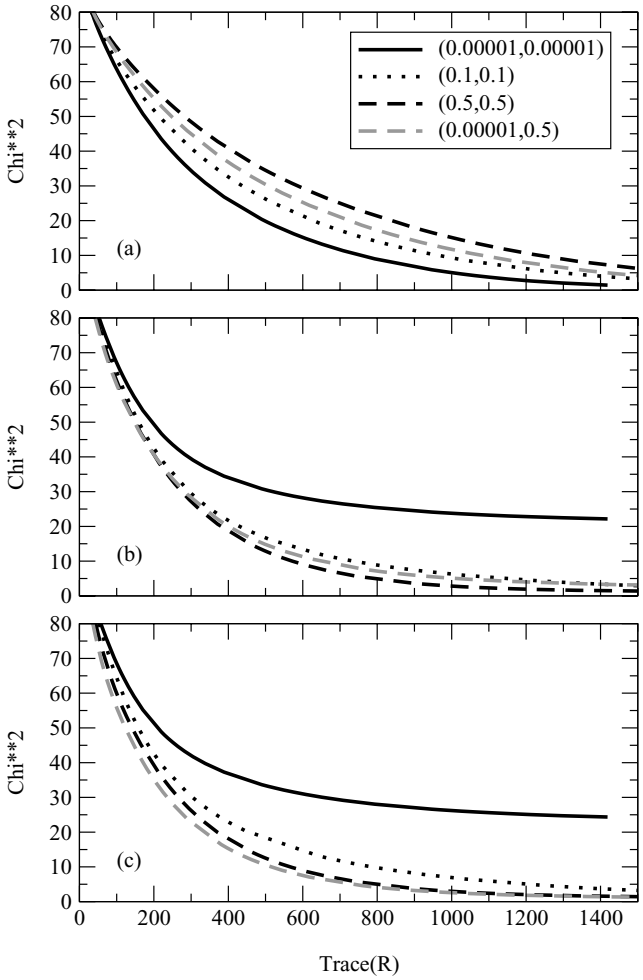

Figure 2. Misfit curves obtained for various random input models. The data coverage used in these simulations corresponds to that shown in Fig. 1. The curves are labelled showing the values of the parameters as (θ_2, θ_4). (a) Isotropic input model; (b) 2ψ and 4ψ input model; (c) 4ψ-only input model.

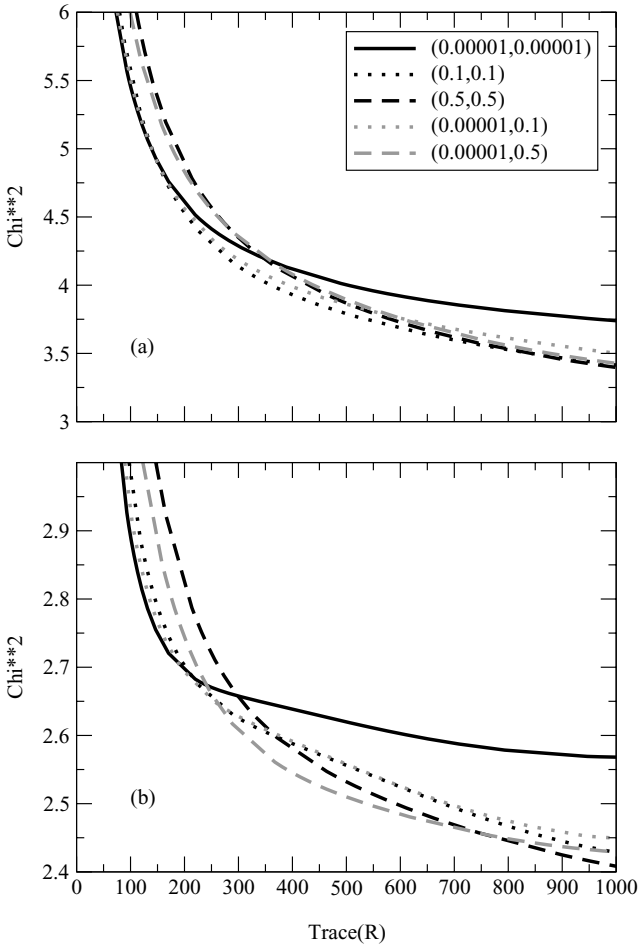

Figure 3. Misfit curves for (a) 40 s Love wave data and (b) 150 s Love wave data.

slightly anisotropic Earth should not give a significant 2ψ term for Love waves in the absence of mode coupling (Montagner & Nataf 1986). In the past, strong 2ψ Love terms have been found (Montagner & Tanimoto 1990) and, if confirmed, most likely means that strong Love–Rayleigh coupling is present. Given the results of the F-test mentioned above, we find that with a sufficiently high degree of confidence our data do not require the inclusion of 2ψ terms.

For Rayleigh waves, all anisotropic misfit curves (Figs 4) are again close together, although there is a slight indication that the data require stronger anisotropy with increasing period. We included a misfit curve with strongly damped 4ψ terms because for some petrological models, it is found that the 2ψ terms are dominant for Rayleigh waves (Montagner & Tanimoto 1991). If the data could distinguish between cases with or without 4ψ terms, this would be a strong petrological discriminant. The F-test shows that the differences between the anisotropic misfit curves are not as significant as the difference with the isotropic case. Nevertheless, at 40 s, the data require with a 95 per cent confidence level a 4ψ term from 750 free parameters onwards. It is less certain whether an overall anisotropic weighting of 0.1 or 0.5 is required. At 150 s, the stronger anisotropy explains the data better with 95 per cent confidence and the neglect of the 4ψ term clearly gives a higher χ^2 as the number of parameters increases. The data thus require a 4ψ term and an increasing strength of anisotropy with period.

5 RESULTS

We constructed azimuthally anisotropic phase velocity maps from our data (58 506 Love wave measurements and 75 515 Rayleigh wave measurements). Although it is clear from the previous paragraph that the data require some degree of anisotropy, the exact strength is difficult to determine. A conservative point of view leads us to choose the smallest significant amount of anisotropy required by the data. Bearing in mind a future depth interpretation, it is most convenient to construct phase velocity models of equal resolution for Love and Rayleigh waves. We finally used $\theta_2 = 10^{-5}$ and $\theta_4 = 0.1$ for Love waves and $\theta_2 = \theta_4 = 0.1$ for Rayleigh waves, although there is an indication that the data need more anisotropy with increasing period. It should be borne in mind that this weighting is put in the cost function but the data still have the possibility to put more anisotropy into longer-period models if needed. λ was adjusted to obtain a total of 800 independently inverted parameters out of the 3405.

Before discussing the models, it is instructive to look at the achieved resolution with the given weighting parameters. The full resolution operator consists of a 3405 $\times$ 3405 matrix, which is difficult to represent. We calculated the full resolution in each case,

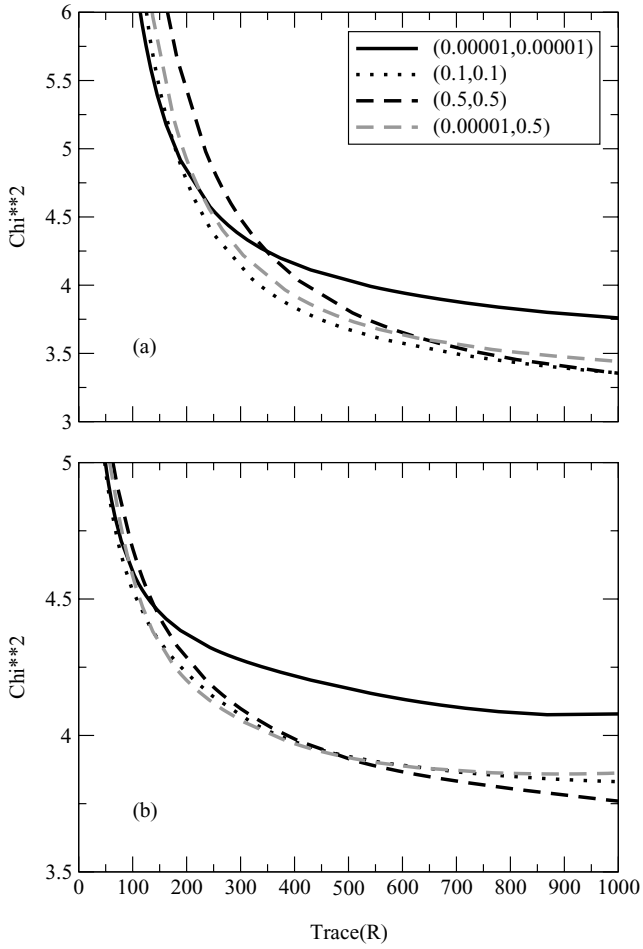

Figure 4. Misfit curves for (a) 40 s Rayleigh wave data and (b) 150 s Rayleigh wave data.

Table 1. Trade-off from resolution operator

Isotropic input model	0ψ	2ψ	4ψ
Love 40 s	0.88	2.3×10^{-15}	8.6×10^{-4}
Love 150 s	0.70	6.8×10^{-15}	2.2×10^{-3}
Rayleigh 40 s	0.88	1.2×10^{-3}	5.8×10^{-4}
Rayleigh 150 s	0.57	4.1×10^{-3}	2.0×10^{-4}

The isotropic input models are from Trampert & Woodhouse (2001). 0ψ lists the output power of the isotropic model part relative to the input power, 2ψ and 4ψ correspond to the respective parts of the azimuthal anisotropy.

but will only comment on two main points of interest, namely the overall lateral resolution and the trade-off between the different azimuthal terms. The overall lateral resolution is calculated from Backus–Gilbert averaging kernels (Trampert & Woodhouse 1995) and is of degree 22 for the isotropic part and degree eight for the azimuthal part. This coincides roughly with values given directly by the trace of the resolution. The important question of whether isotropic structures can give rise to apparent azimuthal anisotropy through inadequate ray coverage is addressed by filtering previously obtained isotropic phase velocity models with the calculated resolution operators. We have chosen the models of Trampert & Woodhouse (2001) because these models and our resolution operators are built from the same number of independent parameters. We calculated the total power of each individual 0ψ, 2ψ and 4ψ output model block relative to the total power of the input model. The results are summarized in Table 1. Regardless of the input model, the trade-off with azimuthal terms is negligible due to our excellent and complementary minor and major arc data coverage. The imperfect isotropic recovery is due to a loss of power in the highest degrees, indicating that part of the small-scale structure in purely isotropic inversions is due to unmodelled azimuthal anisotropy. This results in a lower overall lateral resolution ($L = 22$) compared with a simple isotropic inversion ($L = 28$) for the same number of inverted

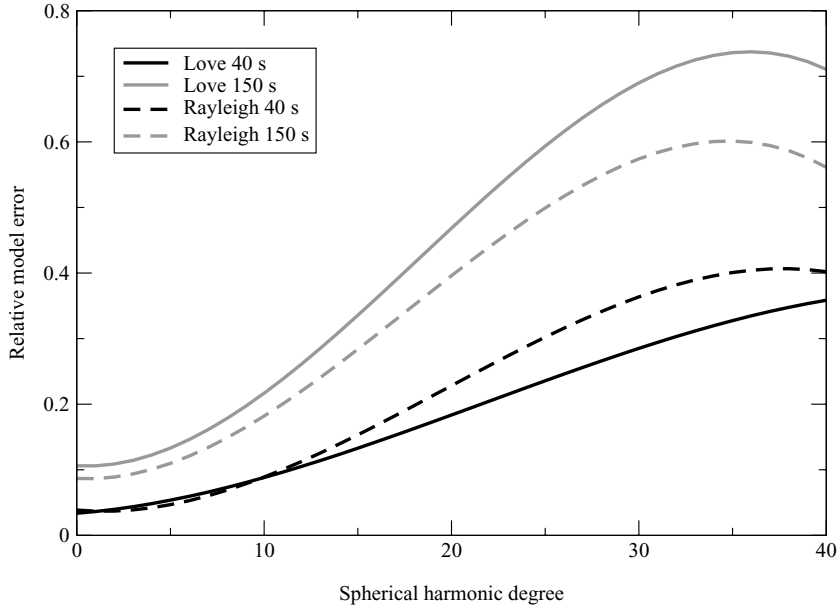

Figure 5. Relative rms error as a function of the spherical harmonic degree for different isotropic phase velocity models. The curves have been smoothed with a cubic regression.

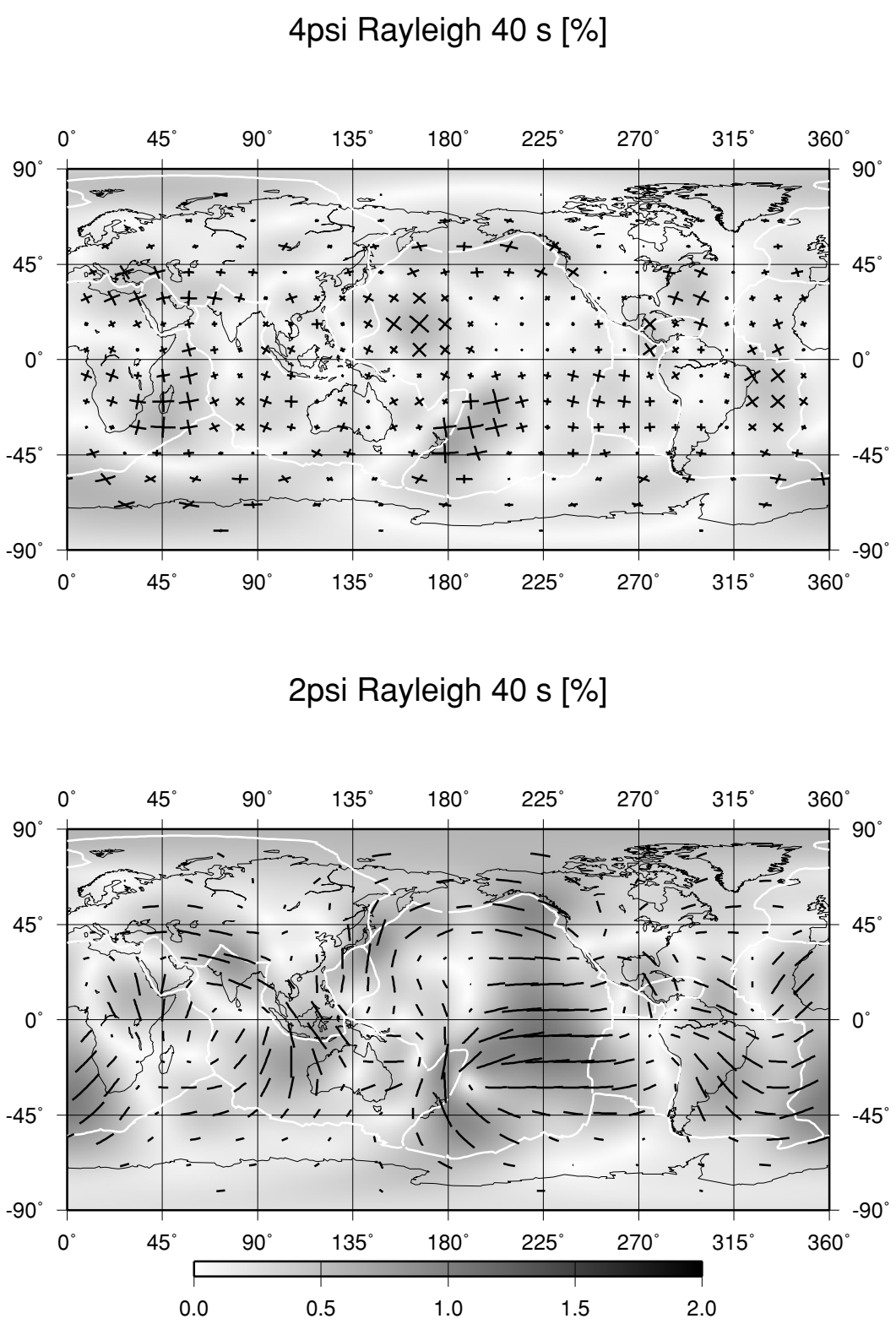

Figure 6. 2ψ (bottom) and 4ψ (top) model for Rayleigh waves at 40 s. The grey-scale in the background corresponds to the peak-to-peak amplitude of anisotropy expressed relative to the average phase velocity calculated from the Preliminary Reference Earth Model (PREM). The black lines represent the fast directions which are also scaled to the amplitude shown in the background. The plate boundaries are plotted in white.

parameters. For the same strength of anisotropy in the cost function, we note that the longer the period, the more gain there is in variance reduction (Figs 3 and 4) and the more loss of power in the highest degrees (Table 1). This is consistent with the findings from the misfit curves that the data require slightly more anisotropy with increasing period. We checked that the lowest degrees remained unchanged.

Another possible influence on the results could come from irregular topography of the major discontinuities within the Earth. To

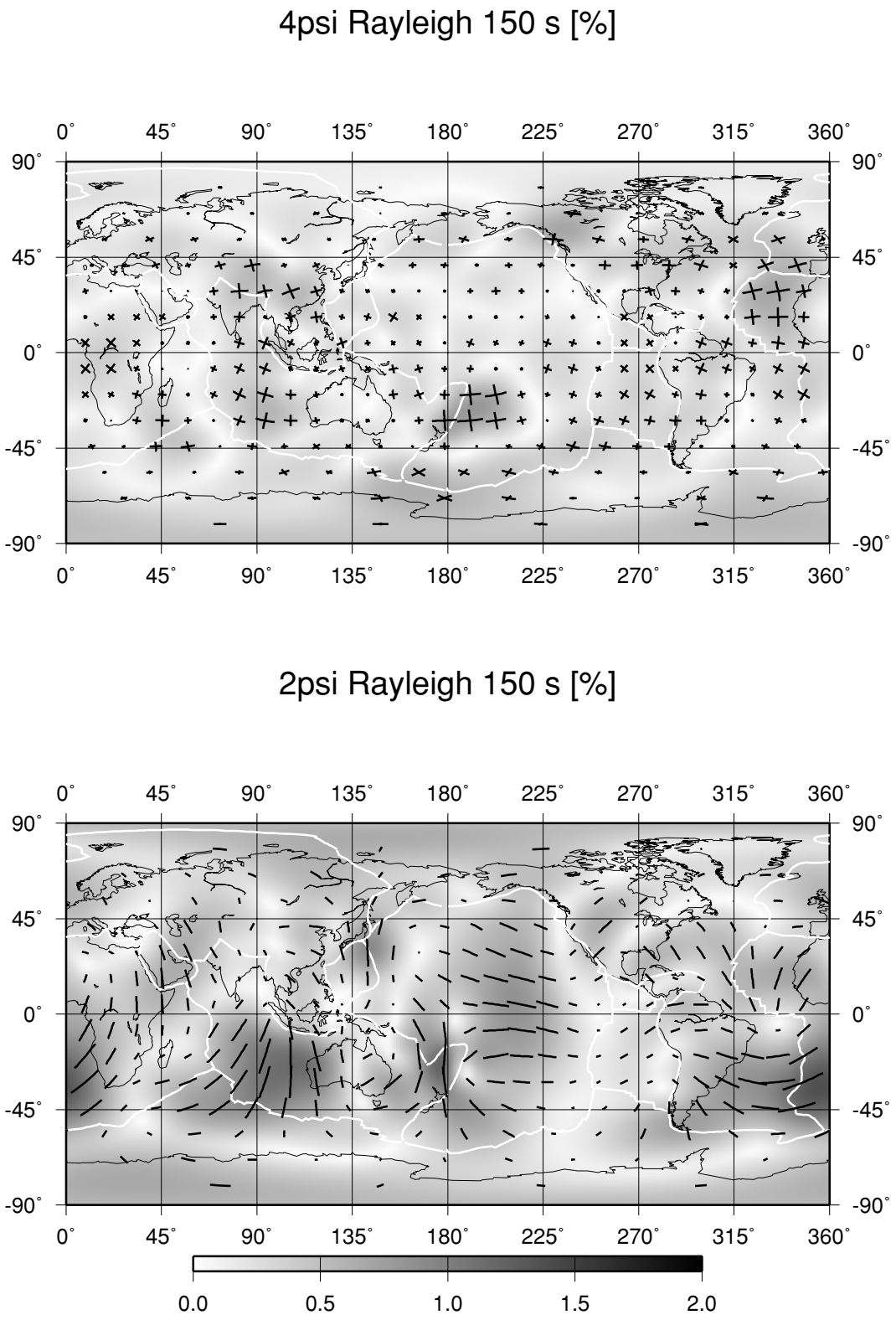

Figure 7. Same as in Fig. 6 but for Rayleigh waves at 150 s.

test this, we corrected our data with the predictions from CRUST5.1 (Mooney *et al.* 1998) and the observed surface topography before inversion. As expected the isotropic models changed accordingly, the 2ψ and 4ψ terms, however, did not change noticeably. Moho depth and topography are the discontinuities with the most pronounced undulations, but we find no significant effects on the azimuthal terms of our models. We interpret this as an indication that undulations in the topography of discontinuities have a first-order effect on the isotropic terms of local phase velocities, but no more than a second-order effect on the azimuthal terms.

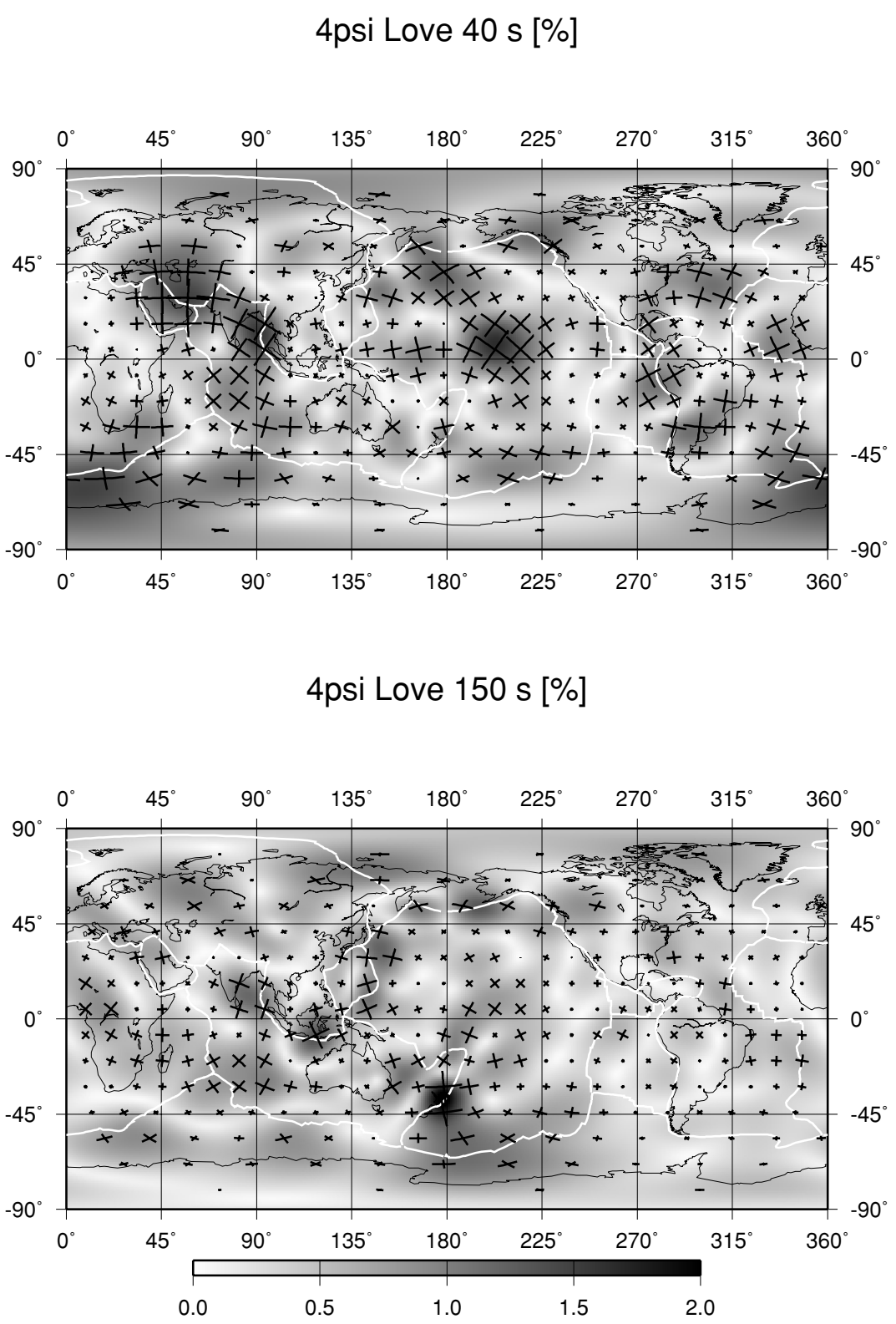

Figure 8. 4ψ model for Love waves at 40 s (top) and 150 s (bottom).

We will not show any results for the isotropic part of the models. We have published several models over the past few years with the aim of distinguishing robust features in the models. The construction of the models is data dependent and not unique because of the need for damping. With our currently published models we can address the variability in the models due to uncertainties in the phase velocity measuring process, data coverage, model parametrization and regularization in the inverse problem. As a quick reminder, we first applied our automatic measuring technique with conservative inbuilt protections, resulting in mainly minor arc data (Trampert &

Woodhouse 1995), which required strong damping in the map construction. In Trampert & Woodhouse (1996), we relaxed the inbuilt protections and measured many major arc data. The resulting maps were built using much less damping. We then refined the measuring technique, starting from aspherical reference models (Trampert & Woodhouse 2001). This resulted in a much better control over the 2π ambiguity. We further cleaned the data set from outliers using cluster analyses. In the present work, we included azimuthal anisotropy in the parametrization having mainly an effect on the higher degrees of the isotropic models. To evaluate the variability in the models thus obtained, we calculate for each spherical harmonic coefficient the mean and variance of the spectral amplitude. In Fig. 5, we plot the ratio of the standard deviation over the mean, giving a relative rms error as a function of the spherical harmonic degree. The relative error increases with increasing period and spherical harmonic degree, indicating that the longer the period and the higher the degree, the more uncertain the models are. As an indication, fixing the acceptable relative model error to 0.3 would mean that models for 40 (150) s become unreliable from degree 25 (15) onwards.

The models for azimuthal anisotropy are plotted in Figs 6–8. In general, for Rayleigh waves, the 2ψ term is stronger (rms amplitude of 0.5 per cent) than the 4ψ term (rms amplitude of 0.25 per cent). The 4ψ term for Love waves is stronger (rms amplitude of 0.5 per cent) than the corresponding Rayleigh wave term. The correlation of 2ψ and 4ψ models at different periods is relatively high (Fig. 9), indicating that the source of anisotropy is shallow, probably lithospheric, but a detailed depth inversion will have to clarify this. For instance, the overall high correlation of the 2ψ Rayleigh terms is dominated by the oceanic part (0.60) compared with a correlation of only 0.16 for continents, suggesting a deeper source of anisotropy beneath continents at least. The dominant degrees in the 2ψ Rayleigh models are two to four. For the 4ψ models the maximum power is found for degree six, slightly shorter wavelength. It is generally observed that the fast directions of the 2ψ Rayleigh terms agree well with directions of plate motions in the oceans (Tanimoto & Anderson 1985; Montagner & Tanimoto 1990). Qualitatively we also see such a correlation, especially fast directions perpendicular to mid-oceanic ridges. While relative plate motions are well constrained, their absolute motion with respect to the underlying mantle is still a matter of debate (Gordon 1995). We considered absolute plate motions in the two most common reference frames: the hotspot reference frame (HS2-NUVEL1 from Gripp & Gordon 1990) and the no-net-rotation reference frame (NNR-NUVEL1 from Argus & Gordon 1991). It has also been suggested that fossil seafloor spreading directions could be important (Nishimura & Forsyth 1989). We obtained these fossil directions from the mapped magnetic anomalies in the oceans. At each point, we calculated the angular difference between the fast direction of the 2ψ Rayleigh term and the local direction of absolute plate motion. Since we are considering directions only, the differences are represented between 0° and 90°. To show the significance of the correlation most clearly, we plotted cumulative distributions and compared them with a set of random angles (Fig. 10). In the oceans, there is no clear overall correlation using the no-net-rotation reference frame or the fossil directions. The corresponding distributions plot close to that of random angles. The hotspot reference shows a clear correlation and we note again the similarity between directions at 40 and 150 s. In continents, the no-net-rotation reference frame again gives no significant correlation, but the hotspot reference frame works remarkably well, especially at 150 s where two-thirds of all directions agree to better than 25° concurring with a recent study beneath Australia (Simons & van der Hilst 2003). This is an interesting observation, because most studies of anisotropy beneath continents rely on shear wave splitting measurements (Silver 1996). It will now be interesting to construct models of azimuthal anisotropy as a function of depth and test several hypothesis concerning the role of plates in the overall mantle flow. The models presented here can be downloaded from ftp://terra.geo.uu.nl/pub/jeannot/twgji02aniso.tar.gz.

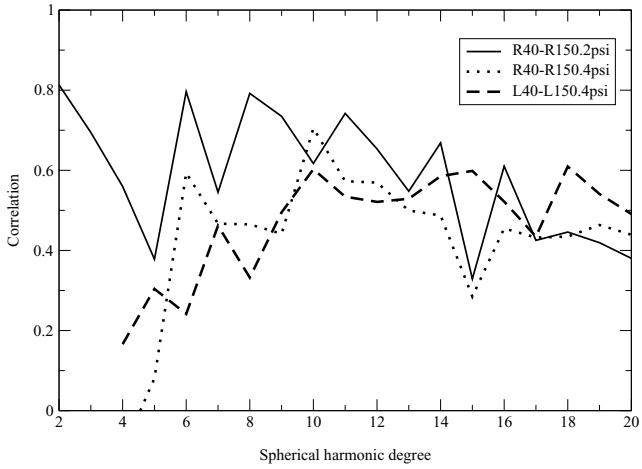

Figure 9. Correlation between different 2ψ and 4ψ models specified in the legend. For 4ψ models, the correlation is low for degrees four and five because the models contain very little power.

6 CONCLUDING REMARKS

We constructed global anisotropic phase velocity maps from more than 100 000 automatically measured phase differences of surface waves between 40 and 150 s. The azimuthal anisotropy is expanded in terms of generalized spherical harmonics, which allows path-averaged phase velocities to be calculated with great ease. This parametrization makes the inverse problem invariant with respect to rotations of the coordinate frame and eliminates singularities associated with the indeterminacy of azimuths at the poles. Great care is taken to determine the strength of anisotropy required by the data. To achieve this we propose a technique based on relative weighting of the different model terms in the cost function associated with the inverse problem. The results show that phase data clearly require azimuthal anisotropy. Including azimuthal anisotropy into phase velocity map constructions reduces the overall lateral resolution of the isotropic part by reducing the power of the highest degrees. This indicates that short-wavelength structure seen in purely isotropic inversion could result from unmodelled azimuthal anisotropy. Concerning azimuthal anisotropy itself, we observe that Love wave data do not require 2ψ terms, whereas Rayleigh wave data need both, 2ψ and 4ψ terms, although the 2ψ term is stronger. Based on correlations, the sources of the observed azimuthal anisotropy are shallow. Only absolute plate motions in the hotspot reference frame show a significant correlation with the fast 2ψ Rayleigh directions.

ACKNOWLEDGMENTS

This research was partly financed by a joint scientific research grant from the Dutch National Science Foundation (NWO) and the British Council. Yanick Ricard provided the fossil sea floor directions based on magnetic anomalies.

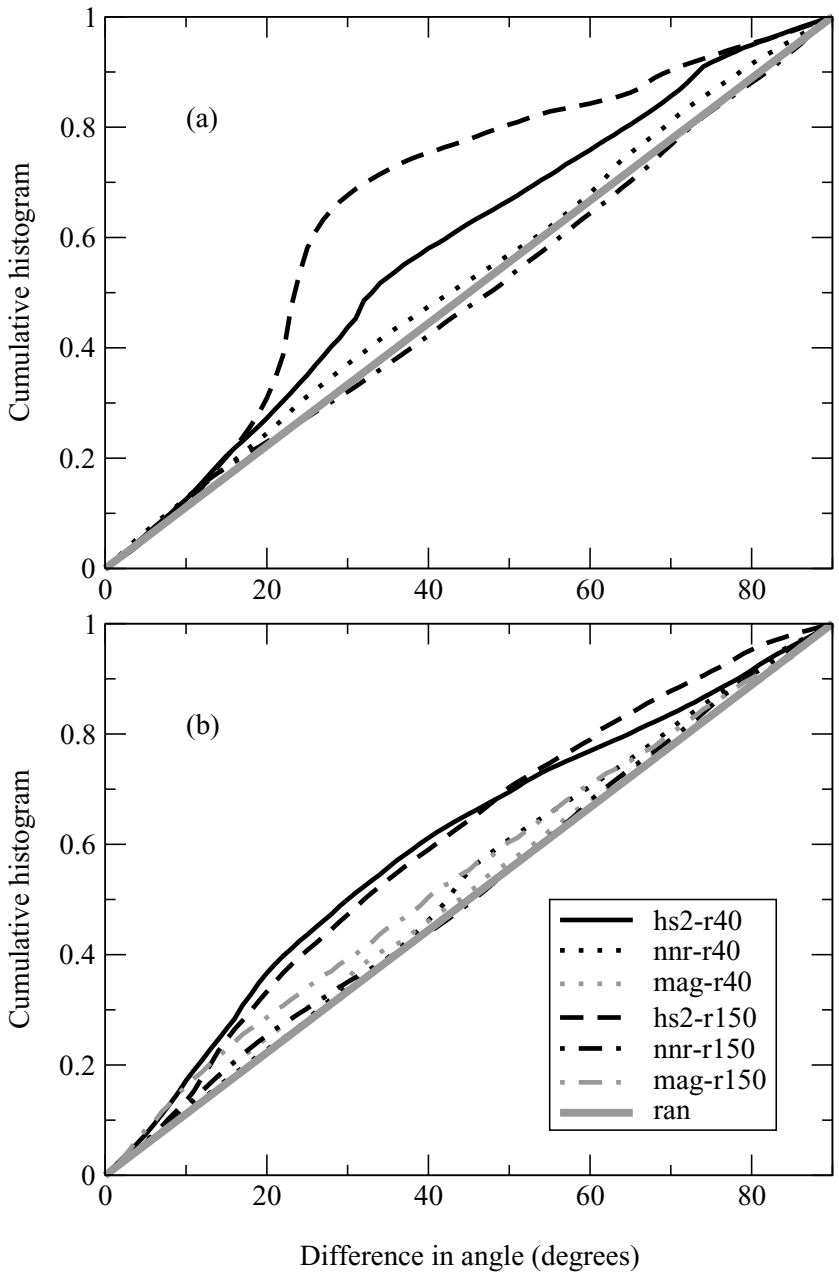

Figure 10. Cumulative distribution of the andular difference between the absolute plate motion and the fast 2ψ Rayleigh directions at 40 and 150 s (a) for continents and (b) for oceans. The plate motions correspond to the models HS2-NUVEL1, NNR-NUVEL1 and the fossil directions deduced from magnetic anomalies. Random angles plot as a straight line in the cumulative graph.

REFERENCES

Aki, K. & Kaminuma, K., 1963. Phase velocity in Japan. Part I. Love waves from the Aleutian shock of March 9, 1957, *Bull. Earthq. Res. Inst.,* **41,** 243–259.

Anderson, D.L., 1961. Elastic wave propagation in layered anisotropic media, *J. geophys. Res.,* **66,** 2953–2963.

Anderson, D.L., 1989. *Theory of the Earth,* Blackwell, Oxford.

Argus, D.F. & Gordon, R.G., 1991. No-net-rotation model of current plate velocities incorporating plate motion model NUVEL-1, *Geophys. Res. Lett.,* **18,** 2038–2042.

Babuška, V & Cara, M., 1991. *Seismic Anisotropy in the Earth,* Kluwer, Dordrecht.

Bevington, P.R. & Robinson, D.K., 1992. *Data Reduction and Error Analyses for the Physical Sciences,* McGraw-Hill, New York.

Dziewonski, A.M. & Anderson, D.L., 1981. Preliminary Reference Earth Model, *Phys. Earth planet. Inter.,* **25,** 297–356.

Ekström, G. & Dziewonski, A.M., 1998. The unique anisotropy of the Pacific upper mantle, *Nature*, **394,** 168–172.

Ekström, G., Tromp J. & Larsen, E.W.F., 1997. Measurements and global models of surface wave propagation, *J. geophys. Res.,* **102,** 8137–8157.

Forsyth, D.W., 1975. The early structural evolution and anisotropy of the oceanic upper mantle, *Geophys. J. R. astr. Soc.,* **43,** 103–162.

Gordon, R.G., 1995. Present plate motions and plate boundaries, in *Global Earth Physics: a Handbook of Physical Constants,* pp. 66–87, ed. Ahrens T.J., American Geophysical Union, Washington

Gripp, A.E. & Gordon, R.G., 1990. Current plate velocities relative to the hotspots incorporating the NUVEL-1 global plate motion model, *Geophys. Res. Lett.,* **17,** 1109–1112.

Harkrider, D.B. & Anderson, D.L., 1962. Computation of surface wave dispersion for multilayered anisotropic media, *Bull. seism. Soc. Am.,* **52,** 321–332.

Hess, H., 1964. Seismic anisotropy of the uppermost mantle under oceans, *Nature*, **203,** 629–631.

Karato, S.-I., 1998. Seismic anisotropy in the deep mantle, boundary layers and the geometry of mantle convection, *Pure appl. Geophys.,* **151,** 565–587.

Larsen, E.W.F., Tromp J. & Ekström G., 1998. Effects of slight anisotropy on surface waves, *Geophys. J. Int.,* **132,** 654–666.

Laske, G. & Masters, G., 1998. Surface wave polarization data and global anisotropic structure, *Geophys. J. Int.,* **132,** 508–520.

Levshin, A.L., Ritzwoller, M.H., Barmin, M.P., Villaseñor, A. & Padgett, C.A., 2001. New constraints on the arctic crust an uppermost mantle: surface wave group velocities, P_n and S_n, *Phys. Earth planet. Inter.,* **123,** 185–204.

McEvilly, T.V., 1964. Central US crust—upper mantle structure from Love and Rayleigh wave phase velocity inversion, *Bull. seism. Soc. Am.,* **54,** 1997–2015.

Montagner, J.-P., 1998. Where can seismic anisotropy be detected in the Earth's mantle? In boundary layers . . . , *Pure appl. Geophys.,* **151,** 223–256.

Montagner, J.-P. & Nataf, H.-C., 1986. A simple method for inverting the azimuthal anisotropy of surface waves, *J. geophys. Res.,* **91,** 511–520.

Montagner, J.-P. & Tanimoto, T., 1990. Global anisotropy in the upper mantle inferred from the regionalization of phase velocities, *J. geophys. Res.,* **95,** 4797–4819.

Montagner, J.-P. & Tanimoto, T., 1991. Global upper mantle tomography of seismic velocities and anisotropies, *J. geophys. Res.,* **96,** 20 337–20 351.

Mooney, W.D., Laske, G. & Masters, G., 1998. CRUST5.1: a global model at 5 degrees by 5 degrees, *J. geophys. Res.,* **102,** 727–748.

Nataf, H.-C., Nakanishi, I. & Anderson, D.L., 1984. Anisotropy and shear velocity heterogeneity in the upper mantle, *Geophys. Res. Lett.,* **11,** 109–112.

Nishimura, C.E. & Forsyth, D.W., 1989. The anisotropic structure in the upper mantle of the Pacific, *Geophys. J.,* **96,** 203–229.

Phinney, R.A. & Burridge, R., 1973. Representation of the elastic–gravitational excitation of a spherical Earth model by generalized spherical harmonics, *Geophys. J. R. astr. Soc.,* **34,** 451–487.

Regan, J. & Anderson, D.L., 1984. anisotropic models of the upper mantle, *Phys. Earth planet. Inter.,* **35,** 227–263.

Romanowicz, B. & Snieder, R., 1988. A new formalism for the effect of lateral heterogeneity on normal modes and surface waves, II: General anisotropic perturbations, *Geophys. J. R. astr. Soc.,* **93,** 91–99.

Silver, P.G., 1996. Seismic anisotropy beneath continents: probing the depths of geology, *Ann. Rev. Earth planet. Sci.,* **24,** 285–432.

Simons, F.J. & van der Hilst, R.D., 2003. Seismic and mechanical anisotropy and the past and present deformation of the Australian lithosphere, *Earth planet. Sci. Lett.,* in press.

Smith, M.L. & Dahlen, F.A., 1973. The azimuthal dependence of Love and Rayleigh wave propagation in a slightly anisotropic medium, *J. geophys. Res.,* **78,** 3321–3333.

Smith, M.L. & Dahlen, F.A., 1975. Correction to 'The azimuthal dependence of Love and Rayleigh wave propagation in a slightly anisotropic medium', *J. geophys. Res.,* **80**, 1923.

Tanimoto, T. & Anderson, D.L., 1984. Mapping convection in the mantle, *Geophys. Res. Lett.,* **11,** 287–290.

Tanimoto, T. & Anderson, D.L., 1985. Lateral heterogeneity and azimuthal anisotropy of the upper mantle: Love and Rayleigh waves 100–250 s, *J. geophys. Res.,* **90,** 1842–1858.

Trampert, J. & Snieder, R., 1996. Model estimations biased by truncated expansions: possible artifacts in seismic tomography, *Science*, **271,** 1257–1260.

Trampert, J. & Woodhouse, J.H., 1995. Global phase velocity maps of Love and Rayleigh waves between 40 and 150 seconds, *Geophys. J. Int.,* **122,** 675–690.

Trampert, J. & Woodhouse, J.H., 1996. High resolution global phase velocity distributions, *Geophys. Res. Lett.,* **23,** 21–24.

Trampert, J. & Woodhouse, J.H., 2001. Assessment of global phase velocity models, *Geophys. J. Int.,* **144,** 165–174.

van Heijst, H.J. & Woodhouse, J.H., 1999. Global high-resolution phase velocity distributions of overtone and fundamental-mode surface waves determined by mode branch stripping, *Geophys. J. Int.,* **137,** 601–620.

Zhang, Y.-S. & Lay, T., 1996. Global surface wave phase velocity variations, *J. geophys. Res.,* **101,** 8415–8436.